
000 THE HIDDEN LATTICE GEOMETRY OF LLMS

001

002

003 **Anonymous authors**

004 Paper under double-blind review

005

006

007 **ABSTRACT**

009 We uncover the *hidden lattice geometry* of large language models (LLMs): a
010 symbolic backbone that grounds conceptual hierarchies and logical operations in
011 embedding space. Our framework unifies the *Linear Representation Hypothesis*
012 with *Formal Concept Analysis* (FCA), showing that linear attribute directions with
013 separating thresholds induce a concept lattice via half-space intersections. This
014 geometry enables symbolic reasoning through geometric meet (*intersection*) and
015 join (*union*) operations, and admits a canonical form when attribute directions are
016 linearly independent. Experiments on WordNet provide empirical evidence that
017 LLM embeddings encode concept lattices and their logical structure, revealing a
018 principled bridge between continuous geometry and symbolic abstraction.

019

020

1 INTRODUCTION

023 Large language models (LLMs) (Achiam et al., 2023; Grattafiori et al., 2024; Mesnard et al., 2024)
024 are surprisingly effective in capturing conceptual knowledge (Petroni et al., 2019; Wu et al., 2023;
025 Lin & Ng, 2022; Xiong & Staab, 2025) and performing logical reasoning, capabilities traditionally
026 associated with symbolic AI. Yet, it remains fundamentally unclear how exactly such conceptual
027 knowledge, including concepts, hierarchies, and their logical semantics, is encoded within the
028 continuous geometry of LLM representation spaces. Unlocking this hidden geometry is crucial not
029 only for interpreting how LLMS representing symbolic knowledge, but also for reliably controlling
030 and steering their inference behavior (Han et al., 2024), a fundamental step for advancing AI safety.

031 To understand concept representations in LLMs, a promising direction is the *Linear Representation*
032 *Hypothesis* (Mikolov et al., 2013b; Park et al., 2025; 2024a; Gurnee & Tegmark, 2024), which
033 posits that semantic features and concepts are encoded as linear directions or subspaces in a model’s
034 embedding space. This idea, rooted in early work on word embeddings (Pennington et al., 2014a),
035 has since been extended to modern LLMs, where such directions can be interpreted as embedding
036 difference, logistic probing, or steering vectors in different contexts (Gurnee & Tegmark, 2024;
037 Nanda et al., 2023; Zhao et al., 2025). Park et al. (Park et al., 2024a) unifies them through *causal*
038 *inner product* that respects the semantic structure of concepts in the sense that causally separable
039 concepts are represented by orthogonal vectors. However, these works mainly focus on exploring the
040 existence of the linearity of (binary) concepts, but offer limited insights for interpreting compositional
041 or set-theoretic semantics such as concept inclusion, concept intersection, and union, which lies at
the heart of symbolic abstraction.

042 Recently, Park et al. (Park et al., 2025) extended the Linear Representation Hypothesis to formalize
043 *categorical concepts* as geometric regions like *polytopes* in the representation space, and show
044 that semantic hierarchy corresponds to orthogonality. However, they model concepts purely in
045 terms of their extensions, that is, as sets of tokens or objects that fall under the category, such as
046 $Y(\text{animal}) = \{\text{predator, bird, dog, ...}\}$. While this extensional view is useful for evaluating
047 membership, it overlooks their intensional nature, i.e., the attributes and relations that ground
048 categories in logic and philosophy, making it difficult to interpret how concepts are related to each
049 others through set-theoretic semantics like concept subsumption, intersection, or union.

050 We draw inspiration from Formal Concept Analysis (FCA) (Ganter et al., 2005), a principled and
051 philosophy-inspired framework that defines concepts through both their instances and their attributes.
052 In FCA, each concept is represented as a pair: an extent (the set of objects) and an intent (the set of
053 shared attributes). For example, the concept *bird* may be defined by attributes such as *can fly*, *has*
feathers, and *lays eggs*, while *eagle* (a bird of prey) refines this category by denoting a subset of

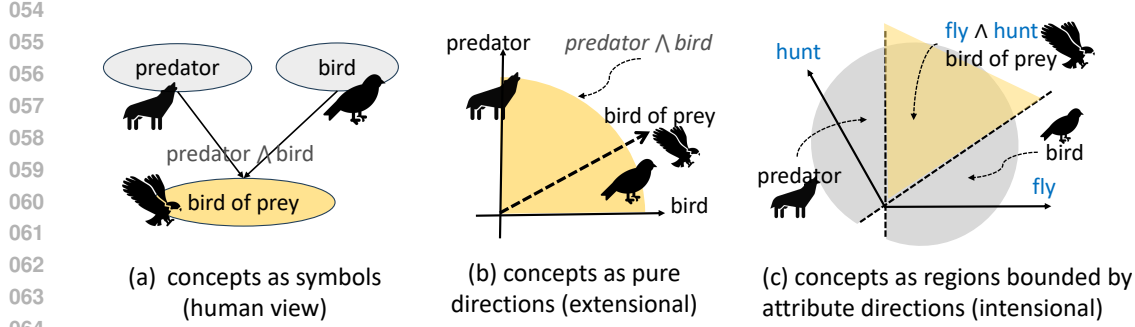


Figure 1: **How LLMs encode conceptual structure.** (a) Humans represent concepts as symbols and compose them using logical operators. (b) Under the standard extensional view, LLMs encode concepts as directions, where subsumption is interpreted through the relative orientation of vectors. (c) Under our intensional view, a concept is represented as the intersection of half-spaces defined by its attributes, and compositional semantics emerges through region intersection and union.

birds with additional features such as can hunt. As Figure 1 shows, unlike extensional view defining concepts as instances, such dual intent-extent view defines concepts as convex regions bounded by their attributes defining them. For example, the concept *bird* may be defined by attributes like *can fly*, *has feathers*, and *lays eggs*, while *eagle* (a bird of prey) refines this category by denoting a subset of birds with additional features such as *can hunt*. This dual formulation naturally induces a concept lattice, because every pair of concepts can be ordered by inclusion of their extents (or, dually, their intents), and any two concepts have a well-defined intersection (their common subconcept) and union (their common superconcept), corresponding to the meet and join operations of the lattice.

In this work, we unify two perspectives on concept representation: the *Linear Representation Hypothesis*, which views semantics as directions in embedding geometry, and *Formal Concept Analysis*, which formalizes concepts through the incidence relation between objects and attributes. **Our key insight is that these views coincide, revealing a hidden lattice geometry in LLMs:** attribute directions correspond to FCA intents, object embeddings to extents, and symbolic abstractions such as subsumption, intersection, and union emerge naturally from the induced closure structure. Building on this connection, we formalize a half-space model of concepts and a projection-based notion of concept inclusion that together recover a lattice geometry from LLM representations. Our contributions are threefold: (i) a theoretical framework linking Linear Representation Hypothesis to FCA via half-space intersections, (ii) a soft inclusion measure and concept algebra (meet/join) defined directly on embeddings, and (iii) empirical evidence on WordNet sub-hierarchies showing that LLM embeddings encode concept lattices, enabling coherent generalization (join) and refinement (meet). These results demonstrate that LLMs implicitly organize conceptual knowledge into a lattice geometry, providing a symbolic backbone for interpretability and controllability.

2 PRELIMINARIES

2.1 LINEAR REPRESENTATION HYPOTHESIS IN LLMs

We consider the autoregressive family of LLMs that predict the next tokens given its context.

Definition 1 (Large Language Model). *An LLM defines a probability distribution over the next token y given a context x via the softmax function $\Pr(y | x) \propto \exp(\lambda(x)^\top \gamma(y))$, where $\lambda : \mathcal{X} \rightarrow \Lambda \simeq \mathbb{R}^d$ maps the input context x to a context embedding vector $\lambda(x)$, and $\gamma : \mathcal{V} \rightarrow \Gamma \simeq \mathbb{R}^d$ maps each vocabulary token y to its unembedding vector $\gamma(y)$.*

This definition involves a *context embedding space* Λ and a *token unembedding space* Γ , which together define the geometry of the softmax distribution. These two spaces can be unified via the *causal inner product* (Park et al., 2024a). Specifically, there exists an invertible matrix $A \in \mathbb{R}^{d \times d}$ and a constant vector $\bar{\gamma}_0 \in \mathbb{R}^d$ such that defining $g(y) := A(\gamma(y) - \bar{\gamma}_0)$ and $\ell(x) := A^{-\top} \lambda(x)$, reparameterizes token and context embeddings into a shared semantic space, where their interaction is captured by the Euclidean inner product $\ell(x)^\top g(y)$. This transformation preserves the model’s output distribution, as the softmax $\Pr(y | x)$ remains invariant under any choice of A and $\bar{\gamma}_0$.

108 In this unified space, Linear Representation Hypothesis states that certain semantic attributes corre-
109 spond to specific directions. There is an explicit definition for binary attributes.

110 **Definition 2** (Linear representation of a binary attribute/concept (Park et al., 2024a)). *A vector*
111 $\bar{\ell}_m \in \mathbb{R}^d$ *is said to linearly represent a binary attribute* $m \in \{0, 1\}$ *if, for all context embeddings*
112 $\ell \in \mathbb{R}^d$, *all scalars* $\alpha > 0$, *and all attributes* $z \neq m$ *that are causally separable from* m , *the following*
113 *conditions hold:*

- 114 • **Attribute activation:** $\Pr(m = 1 | \ell + \alpha \bar{\ell}_m) > \Pr(m = 1 | \ell)$;
- 115 • **Causal selectivity:** $\Pr(z | \ell + \alpha \bar{\ell}_m) = \Pr(z | \ell)$.

118 In other words, moving in the direction $\bar{\ell}_m$ increases the likelihood of the attribute m without affecting
119 any causally unrelated attributes. The direction merely encodes the semantic direction of the attribute,
120 not its strength, as any positive scalar multiple $\alpha \bar{\ell}_m$ has the same qualitative effect.

122 2.2 FORMAL CONCEPT ANALYSIS (FCA)

123 FCA (Ganter et al., 2003) is a mathematical framework for modeling concepts as structured relation-
124 ships between objects and their attributes. Unlike extensional views that define concepts simply as
125 sets of objects (as in (Cowsik et al., 2024)), FCA treats a concept as an intensional abstraction: a set
126 of objects characterized by a common set of attributes. This duality between objects and attributes
127 allows FCA to capture both the semantic content of a concept and its compositional structure. FCA
128 begins with a binary relation between objects and attributes, formalized as a *formal context*:

129 **Definition 3** (Formal context). *A formal context is a triple* (G, M, I) , *where* G *is a finite set of*
130 *objects, M is a finite set of attributes, and $I \subseteq G \times M$ is a binary relation (called the incidence*
131 *relation) such that* $(g, m) \in I$ *indicates that object* $g \in G$ *possesses attribute* $m \in M$.

132 From this, FCA defines concepts as maximal sets of objects and attributes that are mutually consistent:

133 **Definition 4** (Formal concept). *Given a formal context* (G, M, I) , *consider a pair* (A, B) *with*
134 *$A \subseteq G$ and $B \subseteq M$. Define the Galois connections as* $A' := \{m \in M \mid \forall g \in A, (g, m) \in I\}$,
135 *$B' := \{g \in G \mid \forall m \in B, (g, m) \in I\}$. The pair (A, B) is called a formal concept if and only if*
136 *$A' = B$ and $B' = A$, where A is the extent and B is the intent.*

137 The set of formal concepts is partially ordered by inclusion of extents (i.e., $A_1 \subseteq A_2$) or equivalently
138 by reverse inclusion of intents (i.e., $B_2 \subseteq B_1$).

139 **Definition 5** (Concept lattice). *Let (A_1, B_1) and (A_2, B_2) be formal concepts. Then* $(A_1, B_1) \leq_C (A_2, B_2)$ *if and only if*
140 *$A_1 \subseteq A_2$ (equivalently, $B_2 \subseteq B_1$), where \leq_C denotes the partial order*
141 *relationship. Under the partial order \leq_C , the set of all formal concepts forms a complete lattice:*
142 *every subset concepts have a greatest lower bound (meet) and a least upper bound (join).*

145 3 THE LATTICE GEOMETRY IN LLMs

146 We now establish a connection between the Linear Representation Hypothesis and Formal Concept
147 Analysis (FCA), showing that the linear geometry of LLM embeddings gives rise to a concept
148 lattice. The key idea is that each binary attribute can be modeled as a direction in the unified space,
149 with membership approximated by a thresholded inner product. This naturally induces a binary
150 object–attribute relation, from which a formal context and concept lattice can be constructed. We
151 refer to this construction as the *lattice geometry* of LLMs. Fig. 2 illustrates such correspondence.

154 3.1 FROM LINEAR TO LATTICE GEOMETRY

155 **Geometric interpretation of attribute membership.** Under the Linear Representation Hypothesis,
156 semantic attributes are encoded as directions while objects (tokens or contexts) are encoded as vectors.
157 Let $\bar{\ell}_m \in \mathbb{R}^d$ denote the direction for attribute m , and $\mathbf{v}_g \in \mathbb{R}^d$ the embedding of object g . The
158 extent to which g possesses m can be estimated by the projection $\mathbf{v}_g \cdot \bar{\ell}_m$. In the idealized case, there
159 exists a threshold τ_m such that $m(g) = 1 \iff \mathbf{v}_g \cdot \bar{\ell}_m \geq \tau_m$. However, perfect separation rarely
160 holds in practice, so we define a *soft incidence relation*:

$$P_\alpha(m(g) = 1) := \sigma(\alpha \cdot (\mathbf{v}_g \cdot \bar{\ell}_m - \tau_m)), \quad (1)$$

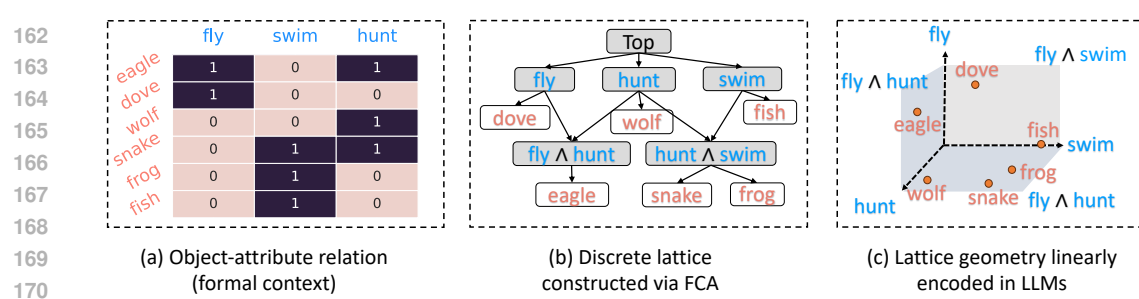


Figure 2: **How FCA connects to the linear lattice geometry of LLMs.** (a) A formal context describing which objects satisfy which attributes. (b) The discrete concept lattice constructed exactly from this formal context. (c) The corresponding lattice geometry encoded in LLM embeddings, where each attribute is represented as a linear direction and each object as a point, and concept composition (meet and join) emerges as intersection or union of half-spaces.

where $\alpha > 0$ is a sharpness parameter controlling the smoothness of the logistic incidence function. A larger α makes the boundary steeper and smaller α makes the boundary smoother. As $\alpha \rightarrow \infty$, this recovers the hard-thresholded case. This assigns each object–attribute pair a fuzzy degree of membership, enabling smoother definitions of concepts.

Theorem 1 (Existence of Lattice Geometry). *Let G be a finite set of objects and M a finite set of attributes. Let $V = \{\mathbf{v}_g \in \mathbb{R}^d \mid g \in G\}$ be object embeddings and $\mathcal{D} = \{\bar{\ell}_m \in \mathbb{R}^d \mid m \in M\}$ attribute directions. Suppose for each $m \in M$ there exists a threshold $\tau_m \in \mathbb{R}$ such that membership is modeled by the soft incidence function above. For any confidence level $\delta \in (0, 1)$, define the binary incidence relation*

$$I_\delta := \{(\mathbf{v}_g, \bar{\ell}_m) \mid P_\alpha(m(g) = 1) \geq \delta\}.$$

Then the induced concept set

$$\mathcal{F}_\delta = \left\{ (X, Y) \mid X = \{\mathbf{v} \in V \mid \forall \bar{\ell} \in Y, (\mathbf{v}, \bar{\ell}) \in I_\delta\}, Y = \{\bar{\ell} \in \mathcal{D} \mid \forall \mathbf{v} \in X, (\mathbf{v}, \bar{\ell}) \in I_\delta\} \right\}$$

satisfies: (i) closure under the Galois connection, and (ii) forms a complete lattice under extent inclusion (equivalently, reverse intent inclusion). Proof is detailed in Appendix B.

Thus, when attributes are encoded as thresholded linear projections, a symbolic concept lattice can be recovered from embedding geometry, capturing semantic abstraction through graded boundaries.

Canonical representation under soft incidence. Theorem 1 allows arbitrary thresholds. We now show that under mild conditions, these thresholds can be absorbed into a global shift of embeddings, yielding a canonical origin-passing form:

Proposition 1 (Canonical representation). *Let each attribute $m_i \in M$ be defined by direction \mathbf{d}_i and threshold τ_i . Let $D \in \mathbb{R}^{k \times d}$ be the matrix with rows \mathbf{d}_i^\top , and $\boldsymbol{\tau} = (\tau_1, \dots, \tau_k)$. If there exists $\mathbf{c} \in \mathbb{R}^d$ such that $D\mathbf{c} = \boldsymbol{\tau}$, then*

$$\sigma(\alpha(\mathbf{v}_g \cdot \mathbf{d}_i - \tau_i)) = \sigma(\alpha((\mathbf{v}_g - \mathbf{c}) \cdot \mathbf{d}_i)) \quad \forall g, i. \quad (2)$$

That is, the probabilities remain invariant under the transformation $\mathbf{v}_g \mapsto \mathbf{v}_g - \mathbf{c}$, reducing the model to a canonical half-space form while preserving the induced lattice. Proof is detailed in Appendix C.

3.2 HALF-SPACE MODEL AND CONCEPT ALGEBRA

Under the canonical representation, where all attribute thresholds have been absorbed via a global shift, each attribute defines an origin-passing half-space in the embedding space. A concept composed of multiple attributes can be interpreted geometrically as the intersection of those half-spaces, i.e., the region where all attribute constraints are simultaneously satisfied.

Definition 6 (Concept as half-space). *Let M be a set of attributes, each represented by a direction $\mathbf{d}_m \in \mathbb{R}^d$. A concept defined by a subset $Y \subseteq M$ corresponds to the set of object embeddings that satisfy all associated directional constraints:*

$$\mathcal{R}(Y) := \{ \mathbf{v} \in \mathbb{R}^d \mid \mathbf{v} \cdot \mathbf{d}_m \geq 0 \text{ for all } m \in Y \}. \quad (3)$$

216 Geometrically, $\mathcal{R}(Y)$ is a convex polyhedral cone defined by intersecting origin-passing half-spaces.
 217 However, this definition assumes perfect attribute separation, which may not hold in practice due
 218 to noise, uncertainty, and overlapping concept boundaries in LLM representations. To address this,
 219 we move from a hard region view to a *soft formulation*, where membership is modeled as graded
 220 alignment rather than binary inclusion.
 221

222 **Concept representation via normalized projection profiles.** Given a concept C (e.g., a lexical
 223 term) and its associated context embeddings $\{\mathbf{v}_1, \dots, \mathbf{v}_n\} \subset \mathbb{R}^d$, we define its semantic representa-
 224 tion using the average projection profile over the attribute directions $\{\mathbf{d}_m\}_{m \in M}$. For each attribute
 225 $m \in M$, the projection value is

$$226 \quad \pi_C(m) := \frac{1}{n} \sum_{i=1}^n \mathbf{v}_i \cdot \mathbf{d}_m. \quad (4)$$

227 The resulting projection vector $\pi_C \in \mathbb{R}^{|M|}$ encodes a *soft attribute profile* of C , reflecting how
 228 strongly the concept aligns with each attribute. This can be seen as a continuous analogue of an FCA
 229 intent. To ensure comparability across concepts, all projection vectors are ℓ_2 -normalized.
 230

232 **Concept inclusion as region containment.** With projection profiles in place, we can now define a
 233 graded notion of subsumption between two concepts. Intuitively, a concept A is included in another
 234 concept B if the attributes emphasized by B are also strongly expressed in A . We capture this by a
 235 *soft inclusion score* that evaluates how well A 's profile satisfies the attribute activations of B :
 236

$$237 \quad \text{Inclusion}(A \sqsubseteq B) = \frac{\sum_{m \in M} \phi(\pi_B(m)) \cdot \sigma(\pi_A(m))}{\sum_{m \in M} \phi(\pi_B(m))}, \quad \text{where } \phi(x) = \log(1 + e^x). \quad (5)$$

239 Here, the sigmoid $\sigma(\cdot)$ maps A 's projection value to a soft likelihood of satisfying attribute m , while
 240 the softplus $\phi(\cdot)$ weights attributes according to their salience in B . This formulation smoothly
 241 downweights weakly expressed or inactive attributes in B , while strongly positive ones dominate the
 242 inclusion score. Thus, concept inclusion is modeled not as a strict set-theoretic containment but as a
 243 continuous, geometry-driven compatibility measure between attribute profiles.
 244

245 **Concept Meet and Join.** We operationalize concept algebra in the half-space model by defining
 246 meet and join directly on concept regions $\mathcal{R}(Y)$. Meet is the intersection of regions, while join is the
 247 least region subsuming both concepts, approximated by the conic hull of their defining directions.
 248

249 **Definition 7** (Concept algebra: meet and join). *Let $\mathcal{R}(Y)$ denote the region associated with a concept
 250 defined by attribute set $Y \subseteq M$ (Definition 6).*

- 251 • **Meet (intersection).** For two concepts $A = \mathcal{R}(Y_A)$ and $B = \mathcal{R}(Y_B)$, their meet is the
 252 region satisfying all attributes from both sets $A \wedge B := \mathcal{R}(Y_A \cup Y_B)$. Geometrically, this
 253 corresponds to intersecting the half-spaces that define A and B .
- 254 • **Join (union or generalization).** Their join is the least upper bound in the lattice, i.e., the
 255 most specific concept region that subsumes both A and B . In the half-space model, this
 256 corresponds to the minimal region that covers $\mathcal{R}(Y_A)$ and $\mathcal{R}(Y_B)$: $A \vee B := \mathcal{R}(Y_A) \cup$
 257 $\mathcal{R}(Y_B)$, which can be approximated by the conic hull spanned by the attribute directions of
 258 A and B .

260 **Soft measure of meet/join.** While Definition 7 specifies meet and join geometrically, we also
 261 require a *graded* way to evaluate how well a concept C corresponds to these symbolic operations.
 262

263 **Soft meet/join profiles.** Given two concepts A, B with projection profiles π_A, π_B , we define the
 264 projection profile of their meet and join using fuzzy t -norm/co-norm combinations:
 265

$$266 \quad \pi_{A \wedge B}(m) = \min\{\pi_A(m), \pi_B(m)\}, \quad \pi_{A \vee B}(m) = \max\{\pi_A(m), \pi_B(m)\}. \quad (6)$$

266 **Degrees of inclusion.** The degree to which C is subsumed by the meet or join is
 267

$$268 \quad \deg(C \sqsubseteq A \wedge B) = \text{Inclusion}(C \sqsubseteq A \wedge B), \quad \deg(C \sqsubseteq A \vee B) = \text{Inclusion}(C \sqsubseteq A \vee B), \quad (7)$$

269 where the inclusion function is as defined in Eq. (2).

270 **Degrees of equality.** Soft equality is defined by symmetrizing inclusion with the harmonic mean:
 271

$$\deg(C = A \wedge B) = \frac{2 \text{Incl}(C \sqsubseteq A \wedge B) \cdot \text{Incl}(A \wedge B \sqsubseteq C)}{\text{Incl}(C \sqsubseteq A \wedge B) + \text{Incl}(A \wedge B \sqsubseteq C)}, \quad (8)$$

$$\deg(C = A \vee B) = \frac{2 \text{Incl}(C \sqsubseteq A \vee B) \cdot \text{Incl}(A \vee B \sqsubseteq C)}{\text{Incl}(C \sqsubseteq A \vee B) + \text{Incl}(A \vee B \sqsubseteq C)}. \quad (9)$$

277 4 EVALUATION

279 In this section, we empirically evaluate the extent to which the linear structure of LLM embeddings
 280 induces a lattice geometry over concepts. We focus on testing the two core assumptions underlying
 281 our framework: 1) **Existence of half-space model:** How well do the linear representations of binary
 282 attributes recover the ground-truth formal context? 2) **Existence of lattice geometry in LLMs:** Does
 283 the approximated formal context recover a valid partial order set or concept lattice?

284 4.1 DATASET AND EXPERIMENT SETUP

286 **Dataset construction.** We construct five object–attribute datasets derived from the WordNet hi-
 287 erarchy. Three datasets correspond to physical domains (**WN-Animal**, **WN-Plant**, **WN-Food**),
 288 and two correspond to abstract domains (**WN-Event**, **WN-Cognition**). Each dataset represents a
 289 distinct semantic domain. Statistics of datasets are shown in Table 4 in the Appendix. For each
 290 domain, we extract all concept terms that fall under the corresponding hierarchy using the WordNet
 291 `is_a` (hypernym) relation. We expand each concept by retrieving its synonyms and hyponyms to
 292 ensure lexical coverage and semantic granularity. Since WordNet does not provide explicit attribute
 293 annotations, we use a large language model (GPT-4o) to generate the attribute schema and populate
 294 the object–attribute matrix. Specifically, for each category, we first prompt the model to produce a
 295 concise set of salient binary attributes relevant to classification within the category (e.g., `can fly`,
 296 `has fur`, `lays eggs` for animals). We then use few-shot prompting to annotate each object with
 297 a binary attribute vector. This produces a complete binary incidence matrix, which we treat as the
 298 ground-truth *formal context* for evaluation. We use the WordNet `is_a` relation to define a symbolic
 299 subsumption hierarchy, and treat it as the target concept lattice structure. Using the annotated formal
 300 context and corresponding LLM embeddings for objects and attributes, we evaluate whether the
 301 geometry of the embedding space can reconstruct the symbolic structure implied by the context.

302 **Object embedding** Each object g is represented by aggregating the embeddings of its lexical
 303 synonyms. For every WordNet object g , we retrieve all lemma names in its synset and treat them as
 304 synonymous surface forms. For each synonym string s , we compute its embedding $\text{Emb}(s) \in \mathbb{R}^d$
 305 as the last hidden state of the model averaged across token positions. The final object embedding is
 306 defined as the mean over its synonym embeddings,

$$\mathbf{v}_g := \frac{1}{|\text{Syn}(g)|} \sum_{s \in \text{Syn}(g)} \text{Emb}(s), \quad (10)$$

309 where $\text{Syn}(g)$ denotes the set of lemma names associated with g . For example, the synset of
 310 *German shepherd* includes *{German shepherd, German shepherd dog, German police dog, alsatian}*.
 311 Averaging across these variants reduces lexical noise, stabilizes surface-form effects, and yields a
 312 more faithful representation of the underlying concept rather than a specific phrasing.

314 **Attribute embedding** To estimate the semantic direction associated with each attribute, we apply a
 315 linear discriminative analysis approach using object embeddings labeled as positive or negative with
 316 respect to that attribute. Given a set of positive and negative object embeddings for attribute m , we
 317 first compute the class means $\boldsymbol{\mu}_+$ and $\boldsymbol{\mu}_-$, and the class covariance matrices Σ_+ and Σ_- , estimated
 318 using Ledoit-Wolf shrinkage to improve robustness in high-dimensional settings. We then define the
 319 attribute direction $\bar{\ell}_m$ as the solution to a regularized Fisher separation criterion:

$$\bar{\ell}_m := (\Sigma_+ + \Sigma_- + \lambda I)^{-1} (\boldsymbol{\mu}_+ - \boldsymbol{\mu}_-), \quad (11)$$

321 where $\lambda > 0$ is a small regularization constant to ensure numerical stability. This procedure yields
 322 a direction vector that best separates the positive and negative object clusters in embedding space
 323 under a linear discriminant model. The resulting vector $\bar{\ell}_m$ is used as the attribute direction in all
 downstream projections and geometric reasoning.

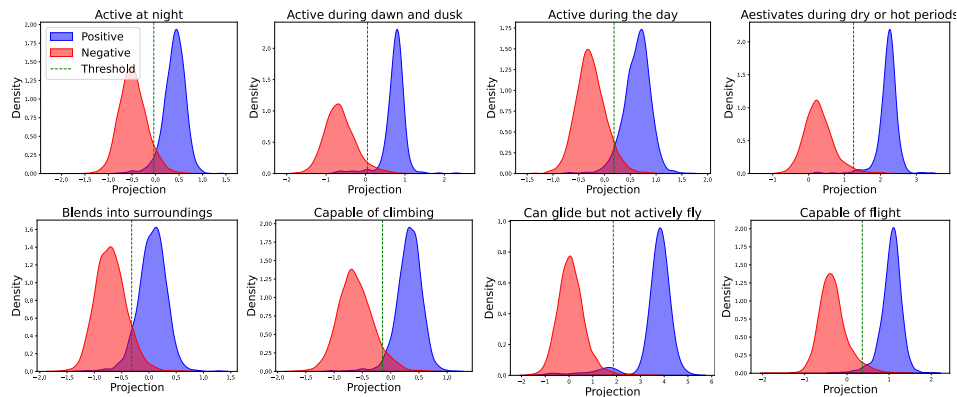


Figure 3: Distribution of projection lengths for positive and negative objects onto the directions of the first eight attributes (sorted alphabetically) in the WN-Animal dataset.

Table 1: Evaluation of recovering concept–attribute relations (formal context). **Bold** denotes the best across models, shading denotes the best within model. All metrics are percentages.

Model	WN-Animal			WN-Plant			WN-Food			WN-Event			WN-Cognition		
	Pre.	Rec.	F1	Pre.	Rec.	F1	Pre.	Rec.	F1	Pre.	Rec.	F1	Pre.	Rec.	F1
LLaMA3.1-8B	Random	49.7	49.6	45.3	50.1	50.1	47.3	50.0	50.0	46.4	50.2	50.2	48.6	50.2	50.1
	Mean	63.7	69.3	63.7	63.7	67.2	63.3	67.2	71.4	68.1	63.7	65.1	63.9	68.4	68.4
	Linear	81.4	84.0	82.5	81.6	82.4	82.4	79.7	80.6	80.1	71.4	71.6	71.5	75.0	75.0
Gemma-7B	Random	49.8	49.7	45.3	50.1	50.1	47.3	50.1	50.1	46.3	49.4	49.3	47.8	50.1	50.1
	Mean	53.5	55.2	50.1	53.5	54.4	51.3	53.7	55.1	51.2	53.3	53.8	52.2	56.4	56.4
	Linear	82.0	84.8	83.2	82.3	84.3	83.2	79.2	80.9	80.0	71.1	71.7	71.4	75.4	75.4
Mistral-7B	Random	49.4	49.2	45.0	50.3	50.4	47.5	49.5	49.5	45.5	50.5	50.6	49.0	49.4	49.3
	Mean	62.2	67.1	62.0	61.9	64.9	61.4	62.4	66.6	62.1	57.2	58.1	56.5	63.3	63.3
	Linear	80.6	83.4	81.8	80.8	82.8	81.7	77.6	78.9	78.2	69.7	69.8	69.7	74.2	74.1

Threshold estimation Given an attribute direction $\bar{\ell}_m$, we determine a threshold $\tau_m \in \mathbb{R}$ to separate positive and negative objects along this direction. For each object embedding \mathbf{v}_g , we compute its projection onto the normalized direction, and then calculate the threshold as the average of the mean projections of positive and negative object sets:

$$\tau_m := \frac{1}{2} (\mathbb{E}_{g \in G_+} [\text{Proj}_m(\mathbf{v}_g)] + \mathbb{E}_{g \in G_-} [\text{Proj}_m(\mathbf{v}_g)]), \quad (12)$$

where G_+ and G_- denote the sets of positive and negative objects for attribute m , respectively. This threshold minimizes classification error under the assumption of linear separability and equal cost.

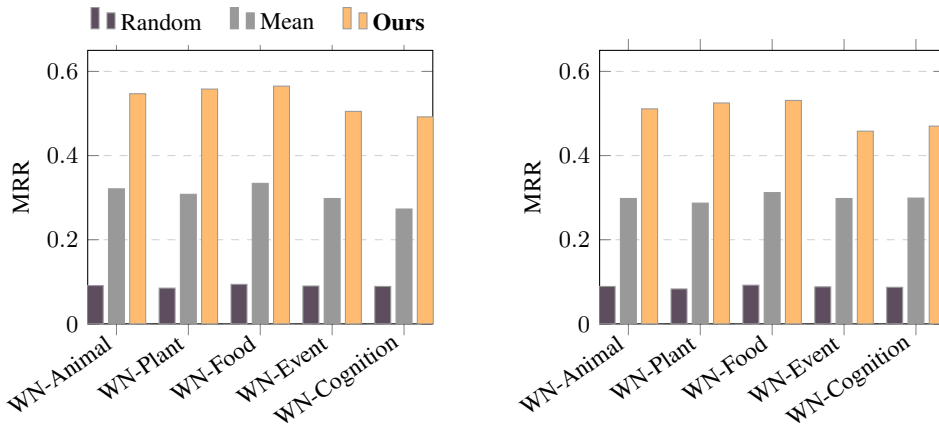
4.2 EXISTENCE OF HALF-SPACE MODEL

We first evaluate whether semantic attributes in LLM embedding space adhere to the half-space model, i.e., whether a single linear direction and threshold can reliably separate objects that possess a given attribute from those that do not. For each attribute m , we estimate a direction \mathbf{d}_m and threshold τ_m using the training set (Section 4.1). Given an object embedding \mathbf{v}_g , we predict whether the object possesses the attribute using a hard decision rule $\hat{m}(g) = \mathbb{I}[\mathbf{v}_g \cdot \mathbf{d}_m \geq \tau_m]$, where $\mathbb{I}[\cdot]$ is the indicator function. We compare this prediction to the ground-truth incidence $m(g) \in \{0, 1\}$ from the annotated formal context. For each attribute, we compute precision, recall, and F1 score, and report averages over all attributes within each dataset.

Results Table 1 reports results for recovering the formal context across five WordNet domains. The *Linear* method achieves the best precision, recall, and F1 on every model and domain, consistently above 78% on physical domains (WN-Animal, WN-Plant, WN-Food) and still strong on the more abstract Event and Cognition domains (above 70%). This demonstrates that LDA-estimated attribute directions align closely with ground-truth concept–attribute structure, even in semantically diffuse domains. The *Mean* baseline performs moderately (59–68% F1), capturing coarse centroids but lacking fine-grained discriminative power. The *Random* baseline stays near chance (45–48%),

378 Table 2: Evaluation of partial order inference from projection-based concept representations. **Bold**
379 denotes the best across models, shading denotes the best within model. All metrics are percentages.
380

381 Model	382 WN-Animal			383 WN-Plant			384 WN-Food			385 WN-Event			386 WN-Cognition			
	387 Pre.	388 Rec.	389 F1	387 Pre.	388 Rec.	389 F1	387 Pre.	388 Rec.	389 F1	387 Pre.	388 Rec.	389 F1	387 Pre.	388 Rec.	389 F1	
383 LLaMA3.1-8B	384 Random	385 52.3	386 43.2	387 47.3	384 Pre.	385 51.1	386 49.5	387 47.6	384 F1	385 25.0	386 50.0	387 33.3	384 Pre.	385 50.2	386 50.2	387 50.2
	384 Mean	385 68.4	386 65.0	387 66.7	384 Pre.	385 64.2	386 63.3	387 63.8	384 F1	385 61.5	386 58.5	387 55.7	384 Pre.	385 60.3	386 57.9	387 59.1
	384 Linear	385 75.9	386 78.3	387 77.1	384 Pre.	385 71.2	386 70.0	387 70.4	384 F1	385 78.1	386 75.9	387 75.4	384 Pre.	385 69.1	386 67.5	387 68.3
385 Gemma-7B	386 Random	387 54.0	388 51.2	389 50.6	386 Pre.	387 52.7	388 50.3	389 49.5	386 F1	387 53.4	388 50.8	389 39.1	386 Pre.	387 49.8	388 50.1	389 49.9
	386 Mean	387 66.2	388 61.0	389 63.4	386 Pre.	387 62.4	388 59.8	389 60.9	386 F1	387 50.7	388 50.7	389 50.6	386 Pre.	387 56.3	388 55.0	389 55.6
	386 Linear	387 74.4	388 76.0	389 75.1	386 Pre.	387 72.9	388 70.1	389 71.4	386 F1	387 76.3	388 75.8	389 75.6	386 Pre.	387 66.2	388 65.1	389 65.6
388 Mistral-7B	389 Random	390 53.3	391 45.9	392 49.3	390 Pre.	391 50.0	392 51.1	393 48.2	390 F1	391 25.0	392 50.0	393 33.3	390 Pre.	391 49.3	392 49.2	393 49.0
	390 Mean	391 66.8	392 63.4	393 64.9	390 Pre.	391 61.2	392 60.0	393 60.5	390 F1	391 56.0	392 55.6	393 54.8	390 Pre.	391 55.7	392 54.3	393 55.0
	390 Linear	391 71.7	392 72.6	393 72.1	390 Pre.	391 65.7	392 60.6	393 57.1	390 F1	391 68.8	392 64.3	393 62.0	390 Pre.	391 62.9	392 60.8	393 61.8



404 Figure 4: Qualitative evaluation (MRR) of concept algebra for Meet (left) and Join (right) operators.
405

406 confirming that attribute recovery is far from trivial and requires meaningful geometric structure.
407 Across models, Gemma-7B and LLaMA3-8B show the strongest linear separability, with Gemma-7B
408 reaching 83.2% F1 on Animal and Plant, and Mistral-7B following closely. Overall, these results
409 provide clear evidence that LLM embeddings support the half-space model of concepts proposed
410 in Section 3.2. Figure 3 further illustrates the separation between positive and negative projection
411 distributions, showing clear margins around the estimated thresholds.

4.3 EXISTENCE OF LATTICE GEOMETRY

415 To test the *existence of lattice geometry*, we use the concept inclusion score defined in Section 3.2,
416 where projection profiles over attribute directions are compared via the soft inclusion formula. This
417 allows us to infer subsumptions directly from embedding geometry without access to ground-truth
418 hierarchies. As Table 2 shows, the LINEAR method consistently outperforms centroid-based (MEAN)
419 and random baselines across all domains, achieving F1 scores up to 77.1 (LLaMA, WN-Animal)
420 and 75.6 (Gemma, WN-Food). These gains demonstrate that discriminatively estimated attribute
421 directions capture intensional information sufficient to recover hierarchical relations: concepts
422 with stronger projection activation on the attributes of another concept are reliably inferred as
423 subconcepts. The empirical alignment between projection-based subsumption and WordNet ground-
424 truth provides strong evidence that LLM embeddings indeed admit a partial order structure, supporting
425 our hypothesis that lattice geometry is embedded within their representation space.

426 **Quantitative evaluation of concept algebra** We quantitatively evaluate the concept algebra using
427 the *degree of equality* metrics in Eq. 8–9. For each WordNet domain, we randomly sample 200
428 concept pairs (A,B) that have at least one shared descendant and one shared ancestor, ensuring
429 well-defined symbolic meets and joins. Gold meets are the lowest shared descendants; gold joins are
430 the least common hypernyms. We compare three approaches: a **Random** scorer, a **Mean** baseline
431 that ranks candidates by similarity to the averaged embeddings of (A, B), and our concept-algebra
operator. For each predicted meet or join, we rank all candidates and report the MRR of the gold

Table 3: Top-10 terms related to the join and meet of selected WordNet concept pairs.

A	B	$A \vee B$	$A \wedge B$
dog	wolf	predator, animal, canine, meat-eater, hunter, wild, mammal, quadruped, pet	dog, hound, puppy, terrier, mutt, beagle, retriever, spaniel, shepherd, pooch
cat	lion	predator, feline, animal, meat-eater, beast, carnivore, hunter, whiskers, mammal, wild	cat, kitten, tiger, panther, leopard, tomcat, feline, cheetah, tabby, lynx
sparrow	robin	avian, songbird, fowl, feathered, finch, beak, chirp, nest, perching, small	sparrow, robin, songbird, warbler, finch, canary, thrush, chickadee, pipit, titmouse
horse	zebra	equid, hooved, animal, ungulate, mammal, quadruped, stallion, beast, herbivore	horse, pony, stallion, mare, foal, filly, mustang, gelding, thoroughbred, colt
carrot	parsnip	root, edible, produce, food, green, vegetable, crunchy, fresh, garden, plant	carrot, parsnip, radish, beet, turnip, tuber, rootcrop, veg, sprout, crop
eagle	falcon	animal, raptor, bird, predator, creature, wingspan, talon, flyer, sky, sharp-eyed	eagle, falcon, hawk, osprey, kestrel, buzzard, kite, harrier, condor, bird of prey

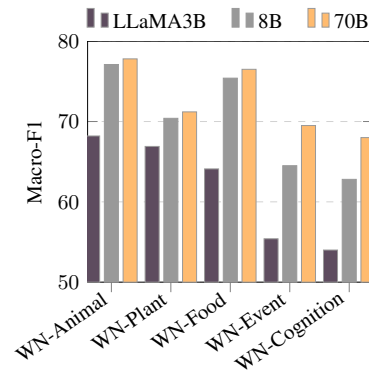
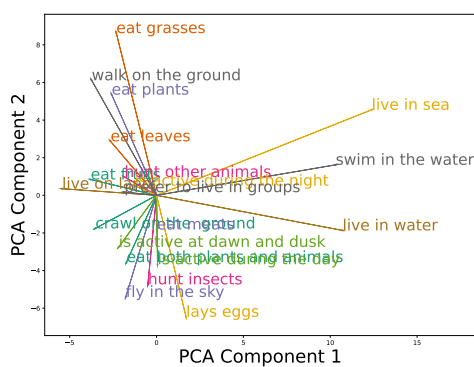


Figure 5: (a) PCA-based visualization of attribute directions in WN-Animal (top 20 most frequent attributes); (b) Performance of LLaMA-3 models of different sizes across WordNet domains.

labels. Figure 4 shows that our method consistently outperforms both baselines, with the largest improvements on physical domains and slightly lower gains on more abstract ones.

Qualitative evaluation of concept algebra We further qualitatively evaluate the concept algebra by randomly selecting concept pairs and inspecting their top-ranked meet and join candidates. As shown in Table 3, the *join* operation ($A \vee B$) reliably returns higher-level abstractions subsuming both inputs (e.g., *predator* for *dog* and *wolf*, or *avian* for *sparrow* and *robin*), mirroring WordNet hypernyms. Conversely, the *meet* operation ($A \wedge B$) produces refined category intersections such as *pony/stallion/foal* for *horse* and *zebra*, or *hawk/osprey* for *eagle* and *falcon*. These examples illustrate that meet and join behave as geometric analogues of set-theoretic conjunction and abstraction, providing qualitative evidence that LLM embeddings encode a coherent latent lattice structure suitable for compositional reasoning.

4.4 ADDITIONAL ANALYSIS

Physical vs. abstract domains Table 1, Table 2, Figure 4, and Figure 5b show a consistent tendency: physical domains (Animal, Plant, Food) achieve relatively better results than abstract domains (Event, Cognition). We conjecture that this is because physical concepts are grounded in concrete, human-perceptual attributes (shape, movement, habitat, function), while abstract concepts rely on more complicated or situational attributes that are less directly encoded in LLMs.

Attribute correlation analysis We visualize the top 20 most frequent attributes in WN-Animal using PCA (Figure 5a) and report their pairwise correlations in the Appendix. The PCA plot reveals coherent semantic clusters, for example, *eat grasses* and *eat plants* appear close together, while *swim in water* and *live in the sea* form a tight group capturing aquatic behaviors. In contrast, attributes associated with unrelated ecological or behavioral properties (e.g., *lays eggs* vs. *live in water*) lie far apart in both the PCA and correlation map. These patterns indicate that the learned attribute directions naturally organize into meaningful semantic subspaces.

486 **Effect of model scaling** We also analyze how lattice-geometry performance scales with model size
487 by comparing LLaMA-3 models from 3B to 70B parameters. As shown in Figure ??, scaling leads to
488 consistent but modest gains on physical domains (WN-Animal, WN-Plant, WN-Food), where even
489 smaller models already capture grounded attributes that structure these categories. In contrast, scaling
490 yields much larger improvements on abstract domains (WN-Event, WN-Cognition), where success
491 depends on representing non-perceptual and relational attributes. This pattern suggests that larger
492 models allocate more capacity to abstract conceptual structure, resulting in more coherent projection
493 geometry in domains less tied to physical properties.

494
495 **5 RELATED WORK AND DISCUSSION**

496 **Conceptual Knowledge in Language Models.** Pretrained language models (LMs) have demonstrated
497 remarkable capabilities in capturing conceptual knowledge (Wu et al., 2023; Lin & Ng, 2022). A
498 variety of methods have been developed to probe such knowledge, most commonly binary probing
499 classifiers (Aspíllaga et al., 2021; Michael et al., 2020) and hierarchical clustering (Sajjad et al., 2022;
500 Hawasly et al., 2024), with validation against human-defined ontologies such as WordNet (Miller,
501 1995). These approaches primarily provide empirical insights into what LMs capture, but they leave
502 open the question of how LMs learn such conceptual structures. Moreover, it has been argued that
503 LMs can develop novel concepts not strictly aligned with existing ontologies (Dalvi et al., 2022),
504 suggesting that ontology-based evaluations may underestimate their conceptual capacity. Xiong &
505 Staab (2025) first show the connection of FCA to language models by define concepts in the context
506 of FCA, but their study is limited to masked language models.

507 **Linear Representation Geometry of Concepts.** A line of research focuses on the geometric nature
508 of concept representations. Several studies suggest that concepts in LMs correspond to distinct
509 directions in activation space (Elhage et al., 2022a; Park et al., 2024a). This linear hypothesis builds
510 on earlier work in distributional semantics and embeddings (Mikolov et al., 2013a; Pennington et al.,
511 2014b; Arora et al., 2016), and has since been connected to multiple notions of linearity, including
512 embedding offsets, probing classifiers, and steering vectors (Park et al., 2024b). Empirical studies
513 have also shown the emergence of polytopes in toy models (Elhage et al., 2022b), pointing to a more
514 structured geometry beyond individual directions. Other theoretical work further explores why linear
515 representations arise, linking them to properties of word embedding models (Arora et al., 2016; 2018)
516 and the implicit bias of gradient descent in LLM training (Jiang et al., 2024).

517
518 **6 CONCLUSION**

519 We presented a new perspective on the geometry of large language models by linking the linear
520 representation of attributes to Formal Concept Analysis (FCA). Our main contribution is the notion
521 of *lattice geometry*, which shows that when attribute directions are treated as separating half-spaces,
522 the resulting object-attribute relation induces a concept lattice. This framework unifies continuous
523 embedding geometry with symbolic abstraction, and provides formal conditions under which logical
524 structure can be recovered from LLM representations. Empirically, we demonstrated on WordNet
525 sub-hierarchies that (i) many attributes are linearly separable, (ii) subsumption can be predicted
526 directly from projection profiles, and (iii) meet and join operations yield meaningful refinements
527 and generalizations. Together, these findings indicate that LLMs encode not only rich conceptual
528 knowledge but also the algebraic backbone of concept lattices. Our results suggest that symbolic
529 abstraction is not an incidental byproduct but a structured geometric property of LLMs. This opens
530 up new directions for neuro-symbolic AI: aligning geometric and symbolic reasoning, enhancing
531 interpretability, and enabling controllable manipulation of concepts in embedding space.

532 **Limitation** Our framework assumes that attributes correspond to approximately linear directions, an
533 assumption supported by prior work on the Linear Representation Hypothesis. However, as noted
534 by Engels et al. (2025), concept types with inherently non-linear, cyclic, or continuously varying
535 structure (for example, months of the year) may violate this linear assumption. Another limitation is
536 that our experimental study focuses on general domains. It is an interesting direction to explore how
537 well the lattice geometry hypothesis holds in domain-specific areas such as biomedical ontologies.

540 **ETHICS STATEMENT**
541

542 This work does not involve human subjects or sensitive personal data. Our experiments are conducted
543 on publicly available lexical resources (WordNet) and pretrained LLM embeddings. We follow the
544 ICLR Code of Ethics¹.
545

546 **REPRODUCIBILITY STATEMENT**
547

548 We have made efforts to ensure the reproducibility of our results. The formal definitions, theo-
549 rems, and proofs are fully detailed in the main text and appendix. Experimental settings, dataset
550 construction (WordNet sub-hierarchies and attribute annotation), attribute direction estimation, and
551 evaluation metrics are described in Section 4. Detailed proofs are provided in the Appendix. Code
552 for reproducing the experiments, including dataset processing and evaluation, are uploaded and will
553 be made available in the supplementary materials.
554

555 **REFERENCES**
556

557 Josh Achiam, Steven Adler, Sandhini Agarwal, Lama Ahmad, Ilge Akkaya, Florencia Leoni Aleman,
558 Diogo Almeida, Janko Altenschmidt, Sam Altman, Shyamal Anadkat, et al. Gpt-4 technical report.
559 *arXiv preprint arXiv:2303.08774*, 2023.
560

561 Sanjeev Arora, Yuanzhi Li, Yingyu Liang, Tengyu Ma, and Andrej Risteski. A latent variable model
562 approach to pmi-based word embeddings. *Transactions of the Association for Computational
563 Linguistics*, 4:385–399, 2016.

564 Sanjeev Arora, Yuanzhi Li, Yingyu Liang, Tengyu Ma, and Andrej Risteski. Linear algebraic structure
565 of word senses, with applications to polysemy. *Transactions of the Association for Computational
566 Linguistics*, 6:483–495, 2018.
567

568 Carlos Aspíllaga, Marcelo Mendoza, and Alvaro Soto. Inspecting the concept knowledge graph
569 encoded by modern language models. In *ACL/IJCNLP (Findings)*, volume ACL/IJCNLP 2021 of
570 *Findings of ACL*, pp. 2984–3000. Association for Computational Linguistics, 2021.

571 Aditya Cowsik, Kfir Dolev, and Alex Infanger. The persian rug: solving toy models of superposition
572 using large-scale symmetries. *CoRR*, abs/2410.12101, 2024.
573

574 Fahim Dalvi, Abdul Rafee Khan, Firoj Alam, Nadir Durrani, Jia Xu, and Hassan Sajjad. Discovering
575 latent concepts learned in BERT. In *ICLR*. OpenReview.net, 2022.
576

577 Nelson Elhage, Tristan Hume, Catherine Olsson, Nicholas Schiefer, Tom Henighan, Shauna Kravec,
578 Zac Hatfield-Dodds, Robert Lasenby, Dawn Drain, Carol Chen, Roger Grosse, Sam McCandlish,
579 Jared Kaplan, Dario Amodei, Martin Wattenberg, and Christopher Olah. Toy models of
580 superposition. *CoRR*, abs/2209.10652, 2022a.

581 Nelson Elhage, Tristan Hume, Catherine Olsson, Nicholas Schiefer, Tom Henighan, Shauna Kravec,
582 Zac Hatfield-Dodds, Robert Lasenby, Dawn Drain, Carol Chen, et al. Toy models of superposition.
583 *arXiv preprint arXiv:2209.10652*, 2022b.
584

585 Joshua Engels, Eric J. Michaud, Isaac Liao, Wes Gurnee, and Max Tegmark. Not all language model
586 features are one-dimensionally linear. In *International Conference on Learning Representations
587 (ICLR)*, 2025. URL <https://arxiv.org/abs/2405.14860>.

588 Bernhard Ganter, Gerd Stumme, and R Wille. Formal concept analysis: Methods, and applications in
589 computer science. *TU: Dresden, Germany*, 2003.
590

591 Bernhard Ganter, Gerd Stumme, and Rudolf Wille. *Formal concept analysis: foundations and
592 applications*, volume 3626. Springer, 2005.
593

¹<https://iclr.cc/public/CodeOfEthics>

594 Aaron Grattafiori, Abhimanyu Dubey, Abhinav Jauhri, Abhinav Pandey, Abhishek Kadian, Ahmad
595 Al-Dahle, Aiesha Letman, Akhil Mathur, Alan Schelten, Alex Vaughan, et al. The llama 3 herd of
596 models. *arXiv preprint arXiv:2407.21783*, 2024.

597 Wes Gurnee and Max Tegmark. Language models represent space and time. In *ICLR*. OpenReview.net,
598 2024.

599 Chi Han, Jialiang Xu, Manling Li, Yi Fung, Chenkai Sun, Nan Jiang, Tarek F. Abdelzaher, and Heng
600 Ji. Word embeddings are steers for language models. In *ACL (1)*, pp. 16410–16430. Association
601 for Computational Linguistics, 2024.

602 Majd Hawasly, Fahim Dalvi, and Nadir Durrani. Scaling up discovery of latent concepts in deep NLP
603 models. In *EACL (1)*, pp. 793–806. Association for Computational Linguistics, 2024.

604 Yibo Jiang, Goutham Rajendran, Pradeep Ravikumar, Bryon Aragam, and Victor Veitch. On the
605 origins of linear representations in large language models. In *Proceedings of the 41st International
606 Conference on Machine Learning (ICML)*, 2024.

607 Ruixi Lin and Hwee Tou Ng. Does BERT know that the IS-A relation is transitive? In *ACL (2)*, pp.
608 94–99. Association for Computational Linguistics, 2022.

609 Thomas Mesnard, Cassidy Hardin, Robert Dadashi, Surya Bhupatiraju, Shreya Pathak, Laurent Sifre,
610 Morgane Rivière, Mihir Sanjay Kale, Juliette Love, et al. Gemma: Open models based on gemini
611 research and technology. *arXiv preprint arXiv:2403.08295*, 2024.

612 Julian Michael, Jan A. Botha, and Ian Tenney. Asking without telling: Exploring latent ontologies
613 in contextual representations. In *EMNLP (1)*, pp. 6792–6812. Association for Computational
614 Linguistics, 2020.

615 Tomáš Mikolov, Wen tau Yih, and Geoffrey Zweig. Linguistic regularities in continuous space word
616 representations. In *Proceedings of NAACL-HLT*, pp. 746–751, 2013a.

617 Tomás Mikolov, Wen-tau Yih, and Geoffrey Zweig. Linguistic regularities in continuous space word
618 representations. In *HLT-NAACL*, pp. 746–751. The Association for Computational Linguistics,
619 2013b.

620 George A. Miller. Wordnet: A lexical database for english. *Commun. ACM*, 38(11):39–41, 1995.

621 Neel Nanda, Andrew Lee, and Martin Wattenberg. Emergent linear representations in world models
622 of self-supervised sequence models. In *BlackboxNLP@EMNLP*, pp. 16–30. Association for
623 Computational Linguistics, 2023.

624 Narmeen Fatimah Oozeer, Luke Marks, Fazl Barez, and Amir Abdullah. Beyond linear steering:
625 Unified multi-attribute control for language models. In Christos Christodoulopoulos, Tanmoy
626 Chakraborty, Carolyn Rose, and Violet Peng (eds.), *Findings of the Association for Computational
627 Linguistics: EMNLP 2025*, pp. 23513–23557, Suzhou, China, November 2025. Association for
628 Computational Linguistics. ISBN 979-8-89176-335-7. doi: 10.18653/v1/2025.findings-emnlp.
629 1278. URL <https://aclanthology.org/2025.findings-emnlp.1278/>.

630 Kiho Park, Yo Joong Choe, and Victor Veitch. The linear representation hypothesis and the geometry
631 of large language models. *ICML*, 2024a.

632 Kiho Park, Yo Joong Choe, and Victor Veitch. The linear representation hypothesis and the geometry
633 of large language models. In *Proceedings of the 41st International Conference on Machine
634 Learning (ICML)*, 2024b.

635 Kiho Park, Yo Joong Choe, Yibo Jiang, and Victor Veitch. The geometry of categorical and
636 hierarchical concepts in large language models. *ICLR*, 2025.

637 Jeffrey Pennington, Richard Socher, and Christopher D. Manning. Glove: Global vectors for word
638 representation. In *EMNLP*, pp. 1532–1543. ACL, 2014a.

639 Jeffrey Pennington, Richard Socher, and Christopher D. Manning. Glove: Global vectors for word
640 representation. In *Proceedings of the 2014 Conference on Empirical Methods in Natural Language
641 Processing (EMNLP)*, pp. 1532–1543, 2014b.

648 Fabio Petroni, Tim Rocktäschel, Sebastian Riedel, Patrick S. H. Lewis, Anton Bakhtin, Yuxiang Wu,
649 and Alexander H. Miller. Language models as knowledge bases? In *EMNLP/IJCNLP (1)*, pp.
650 2463–2473. Association for Computational Linguistics, 2019.

651
652 Uta Priss. Linguistic applications of formal concept analysis. In *Formal concept analysis: foundations*
653 and *applications*, pp. 149–160. Springer, 2005.

654 Hassan Sajjad, Nadir Durrani, Fahim Dalvi, Firoj Alam, Abdul Rafee Khan, and Jia Xu. Analyzing
655 encoded concepts in transformer language models. In *NAACL-HLT*, pp. 3082–3101. Association
656 for Computational Linguistics, 2022.

657 Weiqi Wu, Chengyue Jiang, Yong Jiang, Pengjun Xie, and Kewei Tu. Do plms know and understand
658 ontological knowledge? In *ACL (1)*, pp. 3080–3101. Association for Computational Linguistics,
659 2023.

660 Bo Xiong and Steffen Staab. From tokens to lattices: Emergent lattice structures in language models.
661 In *The Thirteenth International Conference on Learning Representations*, 2025.

663 Haiyan Zhao, Heng Zhao, Bo Shen, Ali Payani, Fan Yang, and Mengnan Du. Beyond single
664 concept vector: Modeling concept subspace in llms with gaussian distribution. In *The Thirteenth*
665 *International Conference on Learning Representations*, 2025.

667 A USE OF LARGE LANGUAGE MODELS (LLMs)

669 Large language models (LLMs) were used as a writing assistant to polish sentences and improve
670 clarity of exposition. Also, we used LLMs to generate annotations of data used for evaluation. No
671 parts of the research ideation, theoretical development, experimental design, or analysis relied on
672 LLMs. All technical contributions, proofs, and empirical results are the work of the authors.

674 B PROOF OF THEOREM 1

676 We restate the theorem for convenience.

678 **Theorem 2** (Existence of Lattice Geometry). *Let G be a finite set of objects and M a finite set of
679 attributes. Let $V = \{\mathbf{v}_g \in \mathbb{R}^d \mid g \in G\}$ be the set of object embeddings and $\mathcal{D} = \{\bar{\ell}_m \in \mathbb{R}^d \mid m \in
680 M\}$ the set of attribute directions. Fix $\alpha > 0$. For each $m \in M$, let $\tau_m \in \mathbb{R}$ and define the soft
681 incidence probability*

$$682 P_\alpha(m(g) = 1) := \sigma(\alpha(\mathbf{v}_g \cdot \bar{\ell}_m - \tau_m)).$$

683 *For any confidence level $\delta \in (0, 1)$, define the (crisp) incidence relation*

$$684 I_\delta := \{(g, m) \in G \times M : P_\alpha(m(g) = 1) \geq \delta\}.$$

685 *Let \mathcal{F}_δ be the set of pairs (X, Y) with $X \subseteq G$ and $Y \subseteq M$ such that*

$$686 X = Y' := \{g \in G : \forall m \in Y, (g, m) \in I_\delta\} \quad \text{and} \quad Y = X' := \{m \in M : \forall g \in X, (g, m) \in I_\delta\}.$$

688 *Then (i) \mathcal{F}_δ is closed under the Galois connection, and (ii) \mathcal{F}_δ , ordered by extent inclusion (equiva-
689 lently, reverse intent inclusion), forms a complete lattice.*

691 **Plan of the proof.** The probabilistic scoring is only used to induce the crisp relation I_δ . Once I_δ
692 is fixed, the statement becomes a standard FCA result. For completeness, we give a self-contained
693 proof.

694 B.1 GALOIS CONNECTION INDUCED BY I_δ

696 **Lemma 1** (Antitone Galois connection). *Define maps $(\cdot)^\prime : 2^G \rightarrow 2^M$ and $(\cdot)^\prime : 2^M \rightarrow 2^G$ by*

$$698 A' := \{m \in M : \forall g \in A, (g, m) \in I_\delta\}, \quad B' := \{g \in G : \forall m \in B, (g, m) \in I_\delta\}.$$

699 *Then for all $A \subseteq G$ and $B \subseteq M$, we have*

$$700 A \subseteq B' \iff B \subseteq A'.$$

701 *Consequently, both primes are antitone: if $A_1 \subseteq A_2$ then $A_2' \subseteq A_1'$, and if $B_1 \subseteq B_2$ then $B_2' \subseteq B_1'$.*

702 *Proof.* (\Rightarrow) If $A \subseteq B'$, then for any $m \in B$ and any $g \in A$ we have $(g, m) \in I_\delta$, hence $m \in A'$ and
 703 thus $B \subseteq A'$. (\Leftarrow) If $B \subseteq A'$, then for any $g \in A$ and $m \in B$ we have $(g, m) \in I_\delta$, i.e., $g \in B'$,
 704 hence $A \subseteq B'$. \square

706 **Lemma 2** (Closure operators). *The double-prime operators $\phi_G(A) := A''$ on 2^G and $\phi_M(B) := B''$ on 2^M are closures: for all $A \subseteq G$, (i) $A \subseteq A''$ (extensivity), (ii) $A \subseteq B \Rightarrow A'' \subseteq B''$ (monotonicity), and (iii) $(A'')'' = A''$ (idempotence). Analogous properties hold on 2^M .*

710 *Proof.* Extensivity: $A \subseteq A''$ follows from Lemma 1 with $B = A'$: $A \subseteq (A')' = A''$. Monotonicity:
 711 $A \subseteq B \Rightarrow B' \subseteq A'$ (antitone), hence $A'' = (A')' \subseteq (B')' = B''$. Idempotence: $(A'')'' = ((A')')'' = (A')' = A''$. The 2^M case is symmetric. \square

715 B.2 FORMAL CONCEPTS AS CLOSED PAIRS

717 **Lemma 3** (Characterization of concepts). *A pair (X, Y) with $X \subseteq G$ and $Y \subseteq M$ satisfies $Y = X'$ and $X = Y'$ iff X and Y are closed, i.e., $X = X''$ and $Y = Y''$.*

720 *Proof.* (\Rightarrow) If $Y = X'$, then $X = (X')' = X''$; if $X = Y'$, then $Y = (Y')' = Y''$. (\Leftarrow) If $X = X''$,
 721 set $Y := X'$ so $X = (X')' = Y'$. The converse from $Y = Y''$ is symmetric. \square

724 B.3 LATTICE STRUCTURE AND COMPLETENESS

725 **Proposition 2** (Partial order). *For formal concepts (X_1, Y_1) and (X_2, Y_2) , define*

$$727 \quad (X_1, Y_1) \leq (X_2, Y_2) : \iff X_1 \subseteq X_2 \quad (\text{equivalently } Y_2 \subseteq Y_1).$$

729 *Then \leq is a partial order on \mathcal{F}_δ .*

731 *Proof.* Reflexivity/transitivity follow from \subseteq . Antisymmetry: $X_1 \subseteq X_2$ and $X_2 \subseteq X_1$ imply
 732 $X_1 = X_2$, hence $Y_1 = X'_1 = X'_2 = Y_2$. \square

735 **Proposition 3** (Meets and joins). *For any family $\{(X_i, Y_i)\}_{i \in I}$ of formal concepts,*

$$737 \quad \bigwedge_i (X_i, Y_i) = \left(\bigcap_i X_i, \left(\bigcap_i X_i \right)' \right), \quad \bigvee_i (X_i, Y_i) = \left(\left(\bigcup_i X_i \right)'', \bigcap_i Y_i \right),$$

739 *and both pairs are formal concepts.*

742 *Proof.* Meet: Let $X_* := \bigcap_i X_i$. Then $(X_*, X'_*) \leq (X_i, Y_i)$ for all i . If $(Z, W) \leq (X_i, Y_i)$ for all i ,
 743 then $Z \subseteq X_*$, so $(Z, W) \leq (X_*, X'_*)$.

744 Join: Let $\tilde{X} := (\bigcup_i X_i)''$ (closed by Lemma 2). Then $(X_i, Y_i) \leq (\tilde{X}, \tilde{X}')$ for all i . If $(X_i, Y_i) \leq$
 745 (Z, W) for all i , then $\bigcup_i X_i \subseteq Z$, hence $\tilde{X} \subseteq Z'' = Z$ and $(\tilde{X}, \tilde{X}') \leq (Z, W)$. \square

748 **Corollary 1** (Completeness). *$(\mathcal{F}_\delta, \leq)$ is a complete lattice: every subset has both meet and join as
 749 above.*

751 B.4 DISCUSSION OF THE ROLE OF α AND δ

753 The parameter $\alpha > 0$ only rescales the logits inside σ and does not affect order-theoretic conclusions,
 754 which depend solely on I_δ . The confidence $\delta \in (0, 1)$ controls the incidence monotonically: if
 755 $\delta_1 \leq \delta_2$ then $I_{\delta_2} \subseteq I_{\delta_1}$. Thus increasing δ removes incidences and yields a different (typically
 coarser) concept lattice. The theorem holds for each fixed δ .

Table 4: Statistics of the five WordNet-derived datasets.

Category	WN-Animal	WN-Plant	WN-Food	WN-Event	WN-Cognition
#Objects	7342	7704	2506	1009	2802
#Attributes	100	145	184	60	107
#Hypernyms	7473	8051	2628	1079	3003

C PROOF OF PROPOSITION 1

Proof of Proposition 1. Let $D \in \mathbb{R}^{k \times d}$ have i -th row \mathbf{d}_i^\top and suppose there exists $\mathbf{c} \in \mathbb{R}^d$ with $D\mathbf{c} = \boldsymbol{\tau}$. Then, for each attribute $i \in \{1, \dots, k\}$,

$$\mathbf{d}_i^\top \mathbf{c} = (D\mathbf{c})_i = \tau_i.$$

Hence, for any object embedding \mathbf{v}_g ,

$$(\mathbf{v}_q - \mathbf{c}) \cdot \mathbf{d}_i = \mathbf{v}_q \cdot \mathbf{d}_i - \mathbf{c} \cdot \mathbf{d}_i = \mathbf{v}_q \cdot \mathbf{d}_i - \tau_i.$$

Applying the sigmoid with sharpness $\alpha > 0$ yields

$$\sigma(\alpha(\mathbf{v}_g \cdot \mathbf{d}_i - \tau_i)) = \sigma(\alpha(\mathbf{v}_g - \mathbf{c}) \cdot \mathbf{d}_i),$$

for all g and i , proving that $P_\alpha(m_i(g) = 1)$ is invariant under the global shift $\mathbf{v}_g \mapsto \mathbf{v}_g - \mathbf{c}$. Therefore, the soft-incidence model admits a canonical, origin-passing form without changing any probabilities or the induced incidence relation for a fixed threshold on P_α . \square

Remarks. (i) The condition $D\mathbf{c} = \boldsymbol{\tau}$ is equivalent to $\boldsymbol{\tau} \in \text{rowspace}(D)$. If the rows $\{\mathbf{d}_i^\top\}_{i=1}^k$ are linearly independent (i.e., $\text{rank}(D) = k$) and $k \leq d$, then $\text{rowspace}(D) = \mathbb{R}^k$, so a (generally non-unique) solution \mathbf{c} exists for any $\boldsymbol{\tau}$. (ii) When solutions exist, they are unique up to addition of any vector in $\ker(D)$; all such choices yield the same invariance because $D(\mathbf{c} + \mathbf{z}) = \boldsymbol{\tau}$ for any $\mathbf{z} \in \ker(D)$.

D ADDITIONAL DISCUSSION AND ANALYSIS

Connection to neuro-symbolic methods and interpretability The soft inclusion and meet/join operators introduced in our framework provide differentiable analogues of logical subsumption and concept composition. These scores make it possible to evaluate whether an LLM’s embedding geometry behaves logically within a given domain, offering a practical interpretability tool for assessing whether the model has learned coherent concept structure. In addition, because the operators are fully differentiable, they can be used as logic-guided regularizers that softly enforce symbolic constraints during training. Examples include subsumption, attribute satisfaction, and type consistency. This creates a natural interface with neuro-symbolic learning, where symbolic rules influence geometric representations through regularization.

Our findings also suggest a natural extension of linear steering to multi-attribute steering Ozeer et al. (2025). Whereas standard steering modifies representations along a single attribute direction, lattice geometry enables logical steering. Enforcing two attributes corresponds to moving the embedding toward their meet. Promoting abstraction corresponds to steering toward their join. Negation corresponds to crossing the relevant threshold hyperplane. These operators provide a simple, differentiable, and interpretable way to compose and control conceptual constraints inside LLMs.

Although our experiments focus on WordNet-style taxonomic domains, the framework is broadly applicable to any setting where concepts can be represented by an object–attribute matrix and attribute inclusion induces a partial order. Examples include semantic fields, where words serve as objects and semantic components serve as attributes, and verb classification or speech-act semantics, where verbs are represented by propositional or pragmatic features Priss (2005). In a linguistic setting where constructions or grammatical patterns are annotated with syntactic or morphological features, the resulting feature matrix can be treated as an FCA context and modeled through the proposed half-space formulation. In general, any domain that provides attribute-labeled objects admits the lattice geometry developed in this work without requiring modification.

810
811
812
813
814
815
816
817
818
819
820
821
822
823
824
825
826
827
828
829
830
831
832
833
834
835
836
837
838
839
840
841
842
843
844
845
846
847
848
849
850
851
852
853
854
855
856
857
858
859
860
861
862
863

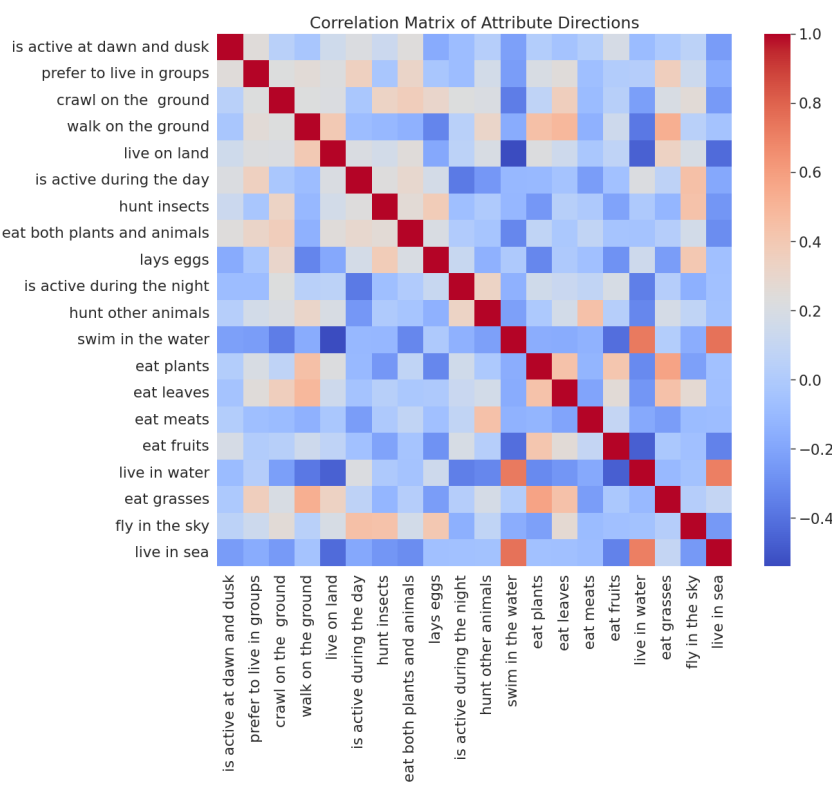


Figure 6: Correlation analysis of attribute directions in the WordNet-Animal dataset.